RESEARCH ARTICLE

Downwash Reduction Drone With Adaptive Rotors and Its 3D Aerodynamic Analysis and Stabilization Control

RYOSUKE MORISHITA[ID], SHIN KAWAI, (Member, IEEE), AND HAJIME NOBUHARA, (Member, IEEE)
University of Tsukuba, Tsukuba, Ibaraki 305-8577, Japan

Corresponding author: Ryosuke Morishita (morishita@cmu.iit.tsukuba.ac.jp)

ABSTRACT When a drone performs physical maneuvers in close proximity to ground objects at extremely low altitudes, the downwash generated significantly impacts the object directly beneath it. In response to this issue, we propose a drone designed to operate at low altitudes while simultaneously creating a windless zone directly beneath the aircraft, thus mitigating its impact on objects below. This entails the development of an H-shaped airframe structure capable of establishing a windless space through the manipulation of rotor angles. Our objective is to formulate a control model for the drone and implement stabilization control. The downwash characteristics of the proposed drone will be methodically investigated through experiments employing a unique 3D airflow measurement system and an operational drone. Visualization of downwash will be generated from the collected wind velocity data, showcasing the potential to create a windless zone when the rotor angle is set to 30° or higher. Additionally, in formulating the control model, we will conduct an extensive search for control parameters that contribute to stabilizing the drone during flight. Through simulation experiments, we aim to demonstrate the feasibility of controlling the drone with rotor angles up to 40° using a conventional controller, utilizing the capabilities of the parameter search algorithm.

INDEX TERMS Drone, downwash, control, H-shaped, weeding.

I. INTRODUCTION

Currently, drones find application in various fields including agriculture, infrastructure inspection, aerial photography, etc. [1], [2], [3], [4]. However, these applications typically involve maintaining a high flight altitude and operating at a distance from the target. This practice is adopted due to the downward airflow generated by the drone, known as downwash (Fig.1 left). Downwash poses challenges when attempting physical actions on objects at low altitudes (2-3 m). For instance, precise weeding encounters challenges as the weeds directly beneath the aircraft are affected by the downwash. Pinpoint weeding is a technique that can eliminate the entire weed by applying a gel-like pesticide directly to the leaves with a drone arm, as shown in Fig.2.

In particular, weeds such as Amaranthus retroflexus (Fig.3) germinate after the middle stage of crop cultivation, proliferating rapidly in fields where the space between ridges is obstructed by crops and tractors, making it inaccessible for people. This technology is garnering attention as the sole method to address these challenging weeds, and its implementation is eagerly anticipated.

Therefore, the research question for this study is: "What defines a drone capable of flying at low altitudes, simultaneously creating a windless space directly below the aircraft to avoid impacting the target?" Therefore, the purpose of this study is to propose an airframe structure for a drone capable of flying at low altitudes that can create a windless space; additionally, this study aims to analyze downwash while developing a control model. To achieve this objective, this study addresses the following three components: The first aspect involves scrutinizing the drone's shape. To effectively
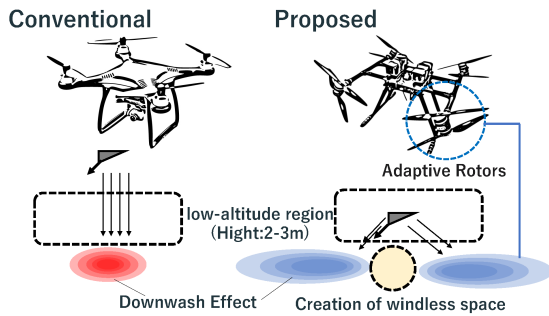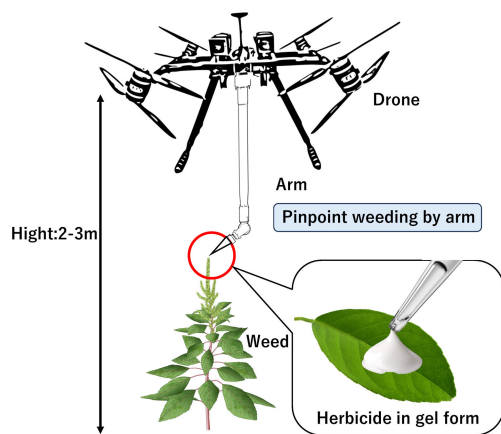
FIGURE 1. Downwash reduction drone.

FIGURE 2. Pinpoint weeding image.

FIGURE 3. Weed conditions requiring pinpoint weeding [5].

reduce downwash, the most impactful method is to adjust the rotor angle that drives the propeller, the primary source of downwash. However, in the case of a variable-rotor type drone with an X-shaped fuselage structure and four rotors, the typical drone configuration, changing the rotor angle towards the center of the fuselage complicates the mechanism.

Therefore, employing an H-shaped structure (Fig.1, right) allows for the variation of the rotor concerning the facing rotor direction, simplifying the mechanism (Fig.4).

The second objective is to elucidate downwash behavior concerning rotor angle. To achieve this, we propose a method

in which anemometers are arranged in an array and can measure in three dimensions. There is no precedent for a study that actually measures such downwash behavior, and this study will reveal downwash behavior for the first time.

The third goal is to determine control parameters based on the rotor angle. To this end, we build a control model and propose a parameter search algorithm based on simulations. Specifically, as the rotor angle changes, parameters likely to affect the drone's operation are adjusted sequentially from among more than a dozen parameters based on conventional drones. Subsequently, parameters that do not overshoot concerning the drone's position output from the simulation are narrowed down. This algorithm searches for parameters for stable flight while doing this for the x- and y-directions.

Notably, there are no research examples of modeling drones that can change the rotor angle, and this research will, for the first time, clarify the limits of the rotor angle that can be controlled by existing controllers.

The following three points elucidate the contributions of this study:

- Verification of the effectiveness of a drone with H-type variable rotors that can create windless space in low altitude flight
- Proposed drone downwash measurement method and clarification of downwash in 3D
- Search for control parameters for stable flight of downwash reduction drone

This paper is organized as follows. Chapter 2 describes related research. Chapter 3 describes a drone with an H-shaped variable rotor and a proposed downwash measurement method, Chapter 4 describes the control model.

II. RELATED WORKS

A. RESEARCH ON WEEDING BY DRONE

Drone weeding has been the subject of numerous studies due to its effectiveness on farms where conventional manual or mechanical weeding methods [6], [7] are impractical [8], [9]. For example, in addition to the research comparing these three methods [10], research on weed detection from images taken by drones for pesticide application has been conducted [11] and path optimization research [12] have been conducted. In addition, research has been conducted on how to prevent the spraying of misty pesticides outside of an area due to disturbances such as wind [13]and research has been conducted on mathematically calculating the optimal method of spraying pesticides [14].

All of the studies used pesticide application and spray-type application methods while maintaining a high drone altitude, and there is room for improvement from the standpoint that these methods are less effective against tall weeds.

B. RESEARCH ON VARIABLE ROTOR DRONES

Research is underway on changing the rotor angle to facilitate more intricate movements than those achievable with conventional drones [15]. This innovation is anticipated to actively contribute to various fields, including inspecting
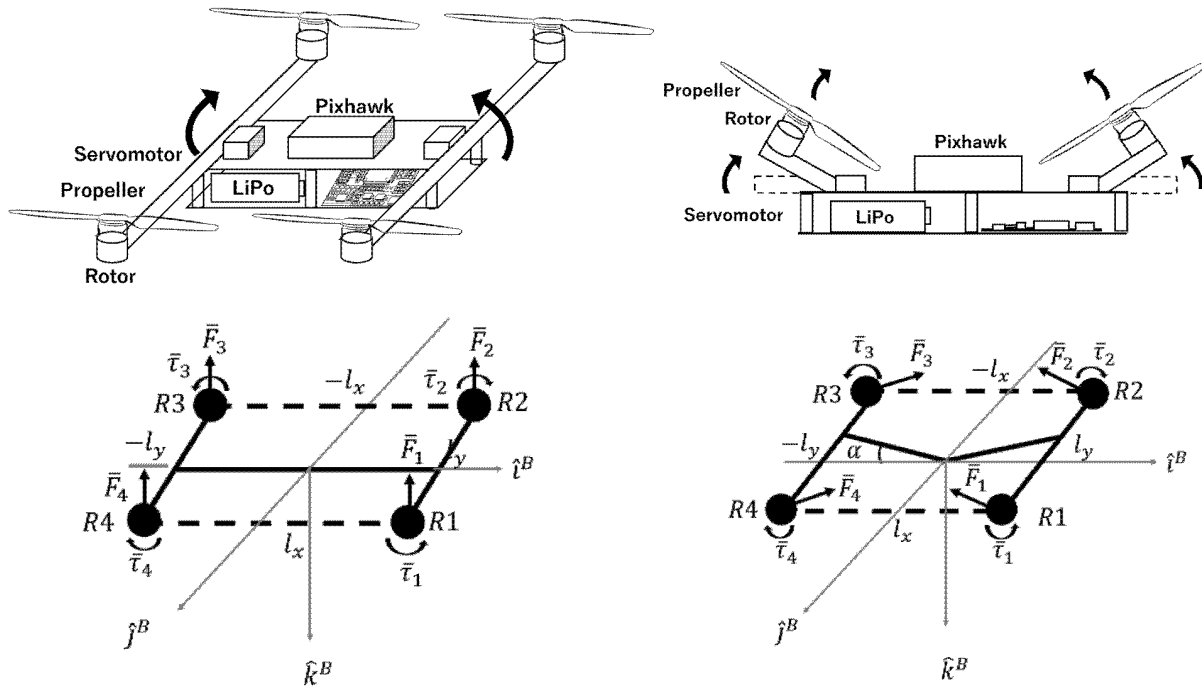
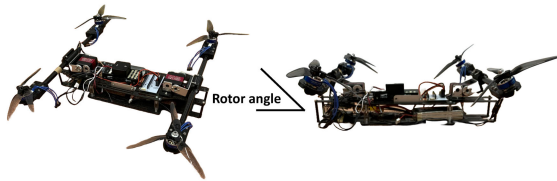**FIGURE 4.** Proposal H-shaped Drone(model).

FIGURE 5. Example of actual realization of the proposed H-type drone.

narrow areas and capturing more realistic images, which were not possible with conventional drones. Notably, the primary aim of this variable-rotor drone is to enable movements not feasible with traditional drones, rather than specifically focusing on downwash reduction. Another existing issue is the lack of explicit information regarding changes in control parameters before and after applying the rotor angle. This study addresses these gaps by specifically varying the rotor angle to mitigate downwash. The control parameters of the controller based on the rotor angle will be clearly outlined, elucidating the relationship between them.

C. RESEARCH ON DRONE DOWNWASH
Due to its significance in drone design and flight, downwash has garnered a significant amount of attention. For example, research on drones that use downwash to spray pesticides [16] and Research has been conducted on aircraft design [17], [18], [19], and control [20], [21], [22], all of which consider the influence of downwash. All of these studies focus on using or analyzing downwash rather than ''reduction'' or creating a windless space directly under the drone. In this sense, the objective of this research to mitigate downwash

and create windless space holds potential to bring innovation to the drone field.

D. POSITIONING OF THIS RESEARCH
In Chapters A to C, no previous studies have been identified on a variable-rotor drone capable of reducing downwash and performing pinpoint weeding. As a result, the primary objective of this study is to introduce an airframe structure for a drone designed to operate at low altitudes, creating a windless space. The study further aims to analyze downwash patterns and construct a comprehensive control model. The envisioned outcome is a drone capable of conducting physical interactions with objects while maintaining low altitudes of $2 - 3$ m.

III. PROPOSAL FOR A 3-D MEASUREMENT METHOD FOR DOWNWASH
A. VARIABLE ROTOR DRONE WITH H-SHAPED MECHANISM
This study introduces a variable-rotor drone employing an H-type mechanism, as illustrated in Fig.4 and Fig.5. Various methods were considered to reduce downwash, including the attachment of a wind blocker directly under the drone and increasing the distance between rotors. Preliminary tests with a wind blocker revealed that it could not effectively reduce downwash due to turbulence. Moreover, increasing the distance between rotors requires approximately 2 m, considering downwash diffusion. This would lead to a larger drone size, making it cumbersome and challenging to handle, especially in agricultural settings where practicality is crucial. Given the potential disincentive of a large-sized drone,

the variable-rotor type was selected as a more viable option. Subsequently, we discuss our deliberations on drone shapes. While a typical drone configuration features four rotors arranged in an X shape, adapting this to a variable-rotor type necessitates setting the rotor angles toward the center of the fuselage, resulting in a complex mechanism. Conversely, the H-type drone boasts a simpler mechanism and is more straightforward to implement. With four rotors installed on the axis of each of the two main rotors, the rotor angle can be easily adjusted by rotating the axis.

B. ANEMOMETER ARRAY FOR 3D MEASUREMENTS

The anemometer array developed in this study is depicted in Fig.6. The framework was created using an aluminum frame. This anemometer array offers two distinct features. Firstly, it allows for the simultaneous measurement of multiple observation points. With four anemometers attached to the array, four locations can be measured concurrently. This facilitates efficient measurements and contributes to a reduction in the overall experiment time. Secondly, the anemometers are designed to be moved freely. Specifically, both the position of each anemometer and the three-dimensional space directly beneath the drone's fuselage can be adjusted independently. This flexibility is achieved by moving the four anemometers vertically or horizontally using the aluminum frame's leg removal mechanism. The utilization of detachable legs for height adjustments serves to prevent obstacles, such as the aluminum frame, from interfering with downwash between the anemometer and the drone. For instance, if the height adjustment were of the sliding type, the pillar portion could disrupt downwash when the anemometer is lowered, potentially impacting the accuracy of measurements. Conversely, employing detachable legs for height adjustments ensures that the space between the drone and the anemometer remains unobstructed, allowing for precise and unimpeded measurements.
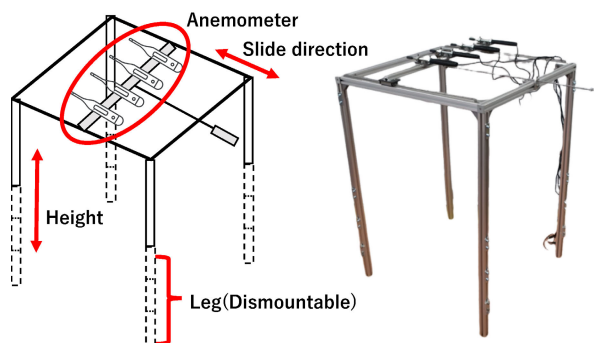

FIGURE 6. Anemometer array. (Left: Blueprint Right: Actual equipment.)

C. DOWNWASH MEASUREMENT DEVICE

The downwash measurement device is illustrated in Figure.7, with the underlying framework constructed using an aluminum frame. To maintain the drone in a state closely
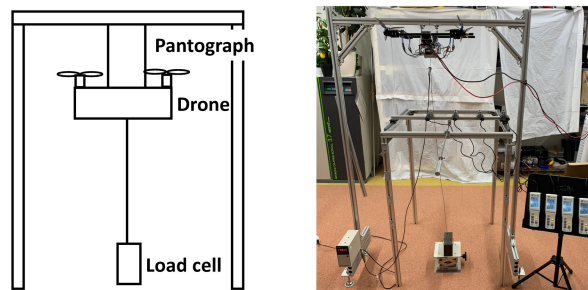

FIGURE 7. Downwash measurement device. (Left: Blueprints Right: Actual equipment.)
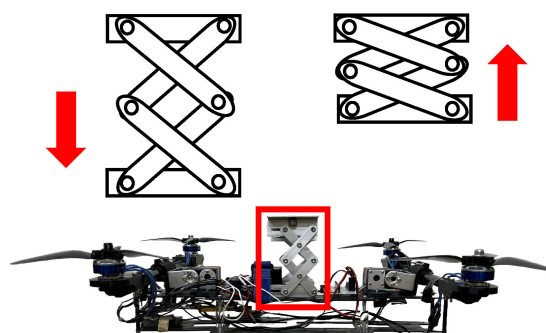

FIGURE 8. Pantograph. (Above: Blueprints Below: Actual equipment.)

resembling flight, a pantograph mechanism (Figure.8) secures the drone in place. This mechanism, attached to the top of the drone, allows the drone vertical freedom of movement. In this setup, when the drone applies thrust and ascends, the pantograph folds down, facilitating the drone's ascent.

Directly beneath the drone, a load cell is positioned. This load cell and the drone are connected to weights on the ground by a string. As the drone ascends, the string is vertically pulled upward, and the resulting force can be measured. This force measurement enables the quantification of the drone's thrust during ascent.

D. DOWNWASH MEASUREMENT EXPERIMENT

Experimental investigations involving downwash measurements were carried out using an apparatus consisting of a variable-rotor drone equipped with the proposed H-type mechanism and an anemometer array. The procedural methodology is visually represented in the algorithm, with detailed elucidation provided in Experimental Procedure and Table.1 for each sequential phase of the experiment.

TABLE 1. Experimental procedure details.

condition	measurement range
Ah(A)	50, 65, 80, 95(cm)
Ra(B)	0, 15, 30, 45(°)
AI(C)	0, 15, 30, 45(cm)

Initially, the determination of the anemometer's elevation, labeled as operation A, was undertaken. Measurements were

acquired at four discrete locations, specifically positioned at distances of 50, 65, 80, and 95 cm from the aerial drone. Subsequent to this, the establishment of the rotor angle, identified as operation B, was ascertained in four incremental steps: 0, 15, 30, and 45°. Furthermore, the quantification of the anemometer position, denoted as operation C, was conducted at 0, 15, 30, and 45 cm beneath the drone.

At each designated measurement juncture, the throttle underwent gradual increments until the load cell registered a value of 100 g, at which point the corresponding anemometer reading was meticulously documented.

Algorithm 1 Experimental Procedure
1: Ah = Anemometer height;
   Ra = Rotor angle;
   AI = Anemometer location;
2: **for** $Ah = 95$ cm to 50 cm step -15 cm **do**
3:     Removing the legs;
4:     **for** $Ra = 0°$ to $45°$ step $15°$ **do**
5:         Change rotor angle;
6:         **for** $Al = 0$ cm to 45 cm step 15 cm **do**
7:             Slide the anemometer;
8:             Increased throttle;
9:         **end for**
10:     **end for**
11: **end for**

Figure 3 illustrates the measurement range of downwash observed from an overhead perspective directly above the drone. Due to the symmetrical nature of the drone used in this study, measurements were exclusively conducted in the first quadrant. By extrapolating and mirroring these findings, it was contemplated that the comprehensive distribution of downwash across the entire space beneath the drone could be ascertained.
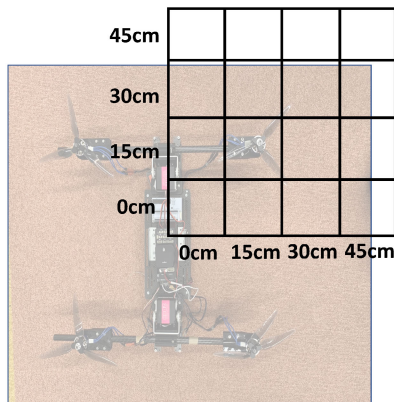

FIGURE 9. Measurement range.

E. RESULTS
Figure.10 illustrates the inversion of experimental outcomes within the first quadrant, presenting the downwash

distribution across the entire area directly beneath the drone. At a rotor angle of 0°, significant wind velocity values were observed in the 15 cm x 15 cm region directly beneath the propeller when the drone was in close proximity to the ground (Figure.11). However, as the distance from the drone increased, the downwash dissipated. Moreover, at a distance of 95 cm from the drone, the wind speed value directly below the aircraft exceeded that below the propeller. This phenomenon may be attributed to the movement of the four rotors during measurement, thereby resulting in the mutual reinforcement of downwash generated by neighboring propellers.

At a rotor angle of 15°, the downwash directly below the drone diminished compared to that at a rotor angle of 0°; however, an adequate windless space was not attained. Conversely, with a rotor angle of 30°, there was an absence of downwash up to 30 cm directly below the drone at a distance of 95 cm, signifying the establishment of a windless space conducive to pinpoint spraying. Similarly, the rotor angle of 45° yielded a windless space suitable for pinpoint spraying.

Subsequently, attention is directed to the throttle value, which increases with the elevation of the rotor angle. It is evident that achieving the required thrust, equivalent to the drone's weight plus 100 g, becomes challenging as rotor angles are heightened. This challenge stems from the realization that only the vertical component of the thrust produced by the propeller contributes to the overall thrust for the aircraft.

TABLE 2. Throttle value according to rotor angle.

Rotor angle(°)	0	15	30	45
Throttle value	10	11	13	20

IV. PROPOSED CONTROL MODEL
A. EQUATION OF MOTION FOR DRONES
Initially, we present the coordinate system (Fig.4) as a foundation for introducing the equations of motion. The primary coordinate system is a right-handed inertial system $\hat{F}^i$, where each axis is represented by the unit vectors $\hat{i}^i, \hat{j}^i, and \hat{k}^i$. These vectors align with the positive directions of magnetic north, east, and gravity, respectively.

The secondary coordinate system is a right-handed dynamic system $\hat{F}^b$ affixed to the aircraft, with the target drone's center of gravity serving as the origin. The unit vectors for this system are denoted by $\hat{i}^b, \hat{j}^b, and \hat{k}^b$, representing the forward, right, and lower directions of the aircraft, respectively. Notably these axes align with the principal axis of inertia.

Building upon the established coordinate systems, we derive the equations of motion. Initially, Newton's equations of motion for inertial systems are expressed as The equations encompass both translational and rotational motion and are formulated as follows:

Drawing upon these considerations, we proceed to derive the equations of motion. Initially, our focus is on Newton's equations of motion, which are formulated for inertial
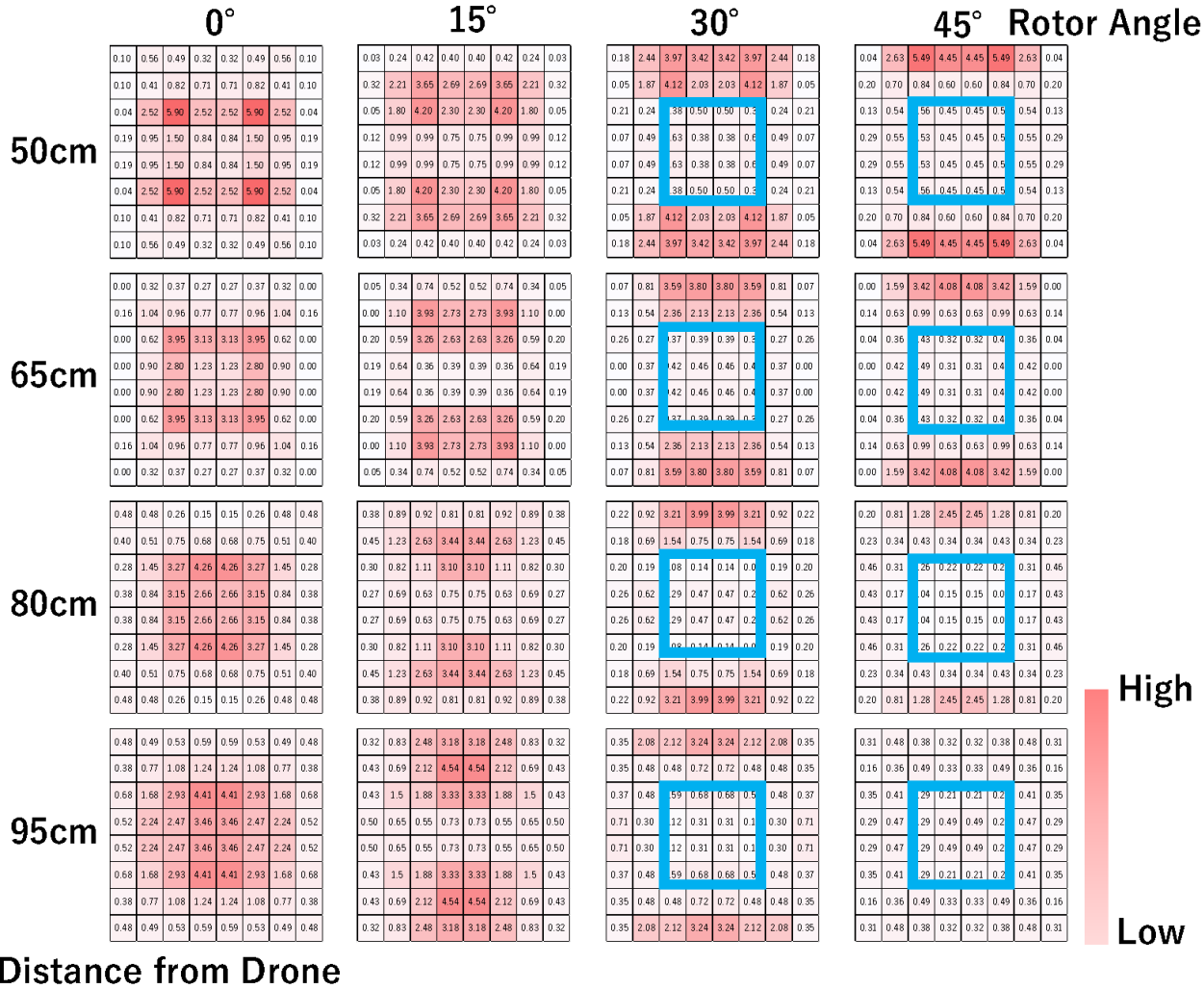
0° 15° 30° 45° Rotor Angle

50cm

65cm

80cm

95cm

High

Low

Distance from Drone

FIGURE 10. Results of downwash measurements. (Wind velocity measurement m/s.)

systems, encompassing both translational and rotational dynamics.

$$M_B \frac{d}{dt} \bar{\boldsymbol{v}}^i(t) = \bar{\boldsymbol{F}}^i(t), \quad (1)$$

$$\frac{d}{dt} \bar{\boldsymbol{h}}^i(t) = \bar{\boldsymbol{T}}^i(t), \quad (2)$$

where $M_B, \bar{\boldsymbol{v}}^i(t), \bar{\boldsymbol{F}}^i(t), \bar{\boldsymbol{h}}^i(t), \bar{\boldsymbol{T}}^i(t)$ denote the mass of the drone, the velocity of the flying object from the fixed coordinate system, the external force, angular momentum, and torque external force on the flying object, respectively.

Equations (1) and (2) are applicable to both conventional and proposed drones, with the left side of the two equations expressed in identical forms. However, the right side exhibits variations between conventional and proposed drones, particularly in terms of the thrust generated by the propeller, external force moments induced by each rotor, and counter torque by the propeller.

Let us consider the rotor angle of the proposed drone as α (Fig.4). In this scenario, the external force acting on the drone,

denoted as $\bar{\boldsymbol{F}}^b(t)$, is composed of the lift force generated by the propeller and the force of gravity on the body.

$$\bar{\boldsymbol{F}}^b(t) = \begin{bmatrix} \sum_{i=1}^{4} n_i \bar{F}_i(t) S_\alpha - M_B g S_\theta \\ M_B g S_\phi C_\theta \\ -\sum_{i=1}^{4} \bar{F}_i(t) C_\alpha + M_B g C_\phi C_\theta \end{bmatrix} \quad (3)$$

When $i = 1, 2$, $n_i = -1$; when $i = 3, 4$, $n_i = 1$. Here, ϕ, θ, ψ represent Z-Y-X Euler angles, g denotes the acceleration due to gravity. Additionally, $S_\theta = \sin(\theta)$ and $C_\theta = \cos(\theta)$.

Subsequently, the external force moments $\bar{\boldsymbol{T}}^b_{Ri}(t)$ arising from the rotor R_i, $i = 1, 2, 3, 4$ are formulated.

$$\bar{\boldsymbol{T}}^b_{Ri}(t) = \begin{bmatrix} (-1)^i l_y \bar{F}_i(t) C_\alpha \\ -n_i \bar{F}_i(t)(l_x C_\alpha + l_z S_\alpha) \\ (-1)^i l_y \bar{F}_i(t) S_\alpha \end{bmatrix}, \quad (4)$$

FIGURE 11. Results. (Anemometer:50 cm,Rotor angle:0°.)

When $i = 1, 2$, $n_i = -1$, and when $i = 3, 4$, $n_i = 1$, and l_x, l_y are the dimensions of the bodies (refer to Fig.4). Next, the counter torque due to the propeller is

$$\bar{\tau}^b = \begin{bmatrix} 0 \\ 0 \\ (-\tau_1 + \tau_2 - \tau_3 + \tau_4)C_\alpha \end{bmatrix}, \quad (5)$$

The counter-torque induced by each propeller is denoted as $\tau_1, \tau_2, \tau_3, \tau_4$, respectively.

Consequently, the aggregate of external force moments is derived by

$$\bar{\boldsymbol{T}}^b(t) = \begin{bmatrix} \bar{T}_1^b \\ \bar{T}_2^b \\ \bar{T}_3^b \end{bmatrix},$$

$$\bar{T}_1^b = l_y C_\alpha \sum_{i=1}^{4} m_i \bar{F}_i(t)$$

$$\bar{T}_2^b = -(l_x + l_z)C_\alpha \sum_{i=1}^{4} n_i \bar{F}_i(t)$$

$$\bar{T}_3^b = (-1)^i \bar{F}_i(t) + (-\tau_1 + \tau_2 - \tau_3 + \tau_4)C_\alpha \quad (6)$$

When $i = 1, 4$, $m_i = -1$, and when $i = 2, 3$, $m_i = -1$. Additionally, for $i = 1, 2$, $n_i = -1$, and for $i = 3, 4$, $n_i = 1$.

Based on the aforementioned conditions, the equation of motion for the drone is expressed as follows:

$$\frac{d}{dt} \begin{bmatrix} \bar{u}(t) \\ \bar{v}(t) \\ \bar{w}(t) \\ J_x \bar{p}(t) \\ J_y \bar{q}(t) \\ J_z \bar{r}(t) \\ \phi(t) \\ \theta(t) \\ \psi(t) \end{bmatrix} = \begin{bmatrix} \bar{u}_1 \\ \bar{v}_1 \\ \bar{w}_1 \\ J_x \bar{p}_1 \\ J_y \bar{q}_1 \\ J_z \bar{r}_1 \\ \phi_1 \\ \theta_1 \\ \psi_1 \end{bmatrix}$$

$$\bar{u}_1 = \sum_{i=1}^{4} n_i \bar{F}_i(t)S_\alpha - M_B g S_\theta - \bar{q}(t)\bar{w}(t) + \bar{r}(t)\bar{v}(t)$$

$$\bar{v}_1 = -\bar{r}(t)\bar{u}(t) + \bar{p}(t)\bar{w}(t) + M_B g S_\phi C_\theta$$

$$\bar{w}_1 = -\sum_{i=1}^{4} \bar{F}_i(t)C_\alpha + M_B g C_\phi C_\theta - \bar{p}(t)\bar{v}(t) + \bar{q}(t)\bar{u}(t)$$

$$J_x \bar{p}_1 = -(J_z - J_y)\bar{q}(t)\bar{r}(t) + l_y C_\alpha \sum_{i=1}^{4} m_i \bar{F}_i(t)$$

$$J_y \bar{q}_1 = -(J_x - J_z)\bar{p}(t)\bar{r}(t) - (l_x + l_z)C_\alpha \sum_{i=1}^{4} n_i \bar{F}_i(t)$$

$$J_z \bar{r}_1 = -(J_y - J_x)\bar{p}(t)\bar{q}(t) + l_y S_\alpha \sum_{i=1}^{4} (-1)^i \bar{F}_i(t)$$
$$+ +(-\tau_1 + \tau_2 - \tau_3 + \tau_4)C_\alpha$$
$$\phi_1 = \bar{p}(t) + (\bar{q}(t)S_\phi + \bar{r}(t)C_\phi)\tan(\theta)$$
$$\theta_1 = \bar{q}(t)C_\phi - \bar{r}(t)S_\phi$$
$$\psi_1 = (\bar{q}(t)S_\phi + \bar{r}(t)C_\phi)\sec(\theta) \quad (7)$$

$\bar{u}$, $\bar{v}$ and $\bar{w}$ are the speed of the drone from the aircraft coordinate system, J_x, J_y and J_z represent the remaining diagonal elements of the moment of inertia tensor, determined by designating each axis of the aircraft coordinate system as the principal axis of inertia. Meanwhile, $\bar{p}(t)$, $\bar{q}(t)$, $and \bar{r}(t)$ denote the angular velocity vectors corresponding to each axis of the aircraft coordinate system.

In equation (7), the segment incorporating the terms S_α, C_α constitutes a significant point of departure between the conventional drone and the proposed drone.

B. CONTROL SIMULATION EXPERIMENTS
This study presents control simulations based on the derived equations of motion, utilizing Pixhawk [23] as the controller. The control model adopts a succinct representation of the drone and Pixhawk(Figure.12). Input to this model comprises the drone's target position and a step function, yielding the 3D position and attitude of the drone as output. Simulink in MATLAB serves as the experimental environment.

Given Pixhawk's extensive array of control parameters, our investigation focused on parameters with potential influence on the drone's behavior. Specifically, attention was directed towards Pixhawk's Position Control P-gain (Pp), as well as the Velocity Control P-gains (Pvx and Pvy) along the X and Y axes. Initially, rotor angle manipulation was conducted, with thirteen angles ranging from 0 to 60° at 5° intervals. Subsequently, Pvx underwent exploration with values of 0.4, 0.3, 0.2, and 0.1. If the overshoot in the drone's position graph remained below 1.5, Pp was scrutinized across five values: 0.15, 0.14, 0.13, 0.12, 0.11and 0.10. During this analysis, parameter combinations preventing overshoot above 1 were sought. Furthermore, with the fixed output of Pp, Pvy operations were conducted to evaluate behavior in the Y direction, following a similar methodology to that applied to Pvx.
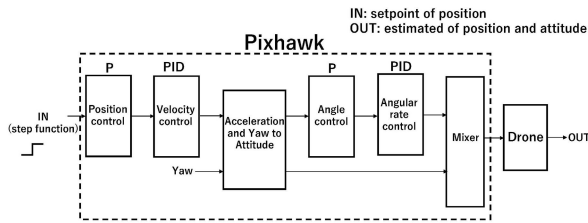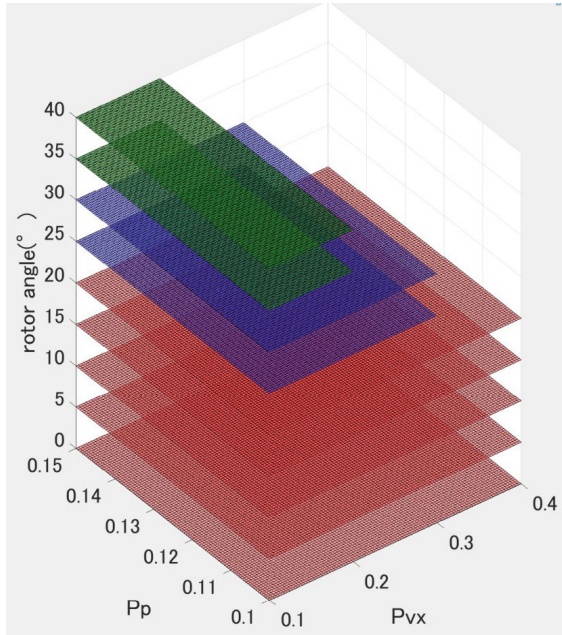
FIGURE 12. Structure of the control scheme.

FIGURE 13. Results of parameter search.

C. RESULTS

The outcomes of the parameter search are illustrated in Figure.13. The plane graph, aligned with the Pvx and Pp axes, signifies the count of Pvx and Pp parameter combinations for each rotor angle. Notably, the observed trend indicates a diminishing area as the increasing rotor angle. Specifically, for rotor angles within the 0° to 20° range, there were 24 parameter combinations, 18 combinations for rotor angles between 25° and 30°, and 12 combinations for rotor angles from 35° to 40°. This reduction implies increased difficulty in achieving stabilization control with higher rotor angles. Notably, for each rotor angle, a singular combination of Pvy and Pp could be identified.

Throughout the experiment, rotor angles were systematically varied from 0° to 60°. However, no viable parameter combinations were discerned beyond the 45° threshold. Potential drone behaviors in these scenarios encompass instances where the drone moves contrary to the target upon initial movement in the X direction, experiences excessive overshooting, or undergoes divergence.

V. CONCLUSION

To address the challenge posed by the downwash of drones affecting objects situated directly beneath the aircraft,

we propose a novel drone design capable of flying at extremely low altitudes while creating a windless zone directly beneath it. To realize this concept, we introduce an H-shaped variable-rotor drone and conduct comprehensive 3D measurements of downwash, coupled with simulations of stabilization control.

Our initial focus is on mitigating downwash, a prominent concern associated with conventional drones. We propose a distinctive drone configuration designed to minimize downwash. Subsequently, we perform 3D measurements of downwash, marking a significant achievement as this research marks the first successful attempt at quantifying downwash behavior. Our findings confirm that an increased rotor angle results in the outward distribution of downwash, effectively diminishing its intensity directly under the drone.

Moving forward, we present a control model and execute control simulation experiments. Through this experimentation, we identify Pixhawk parameters corresponding to rotor angles using our proprietary parameter search algorithm. In the future, subsequent to conducting control simulations incorporating disturbances, we intend to execute real-world flights to ascertain the feasibility of stable flight even when adjusting the rotor angle.

REFERENCES

[1] N. C. Coops, T. R. Goodbody, and L. Cao, "Four steps to extend drone use in research," *Nature*, vol. 572, no. 7770, pp. 433–435, Aug. 2019.

[2] Y. Matsuura, Z. Heming, K. Nakao, C. Qiong, I. Firmansyah, S. Kawai, Y. Yamaguchi, T. Maruyama, H. Hayashi, and H. Nobuhara, "High-precision plant height measurement by drone with RTK-GNSS and single camera for real-time processing," *Sci. Rep.*, vol. 13, no. 1, p. 6329, Apr. 2023.

[3] N. Falco, H. M. Wainwright, B. Dafflon, C. Ulrich, F. Soom, J. E. Peterson, J. B. Brown, K. B. Schaettle, M. Williamson, J. D. Cothren, R. G. Ham, J. A. McEntire, and S. S. Hubbard, "Influence of soil heterogeneity on soybean plant development and crop yield evaluated using time-series of UAV and ground-based geophysical imagery," *Sci. Rep.*, vol. 11, no. 1, p. 7046, Mar. 2021.

[4] R. Nagasawa, E. Mas, L. Moya, and S. Koshimura, "Model-based analysis of multi-UAV path planning for surveying postdisaster building damage," *Sci. Rep.*, vol. 11, no. 1, p. 18588, Sep. 2021.

[5] NPP Organizations. (2020). *Bulletin OEPP EPPO Bulletin Volume50*. [Online]. Available: https://onlinelibrary.wiley.com/doi/full/10.1111/epp.12716

[6] Y. Du, B. Mallajosyula, D. Sun, J. Chen, Z. Zhao, M. Rahman, M. Quadir, and M. K. Jawed, "A low-cost robot with autonomous recharge and navigation for weed control in fields with narrow row spacing," in *Proc. IEEE/RSJ Int. Conf. Intell. Robots Syst. (IROS)*, Sep. 2021, pp. 3263–3270.

[7] A. Ahmadi, M. Halstead, and C. McCool, "BonnBot-I: A precise weed management and crop monitoring platform," in *Proc. IEEE/RSJ Int. Conf. Intell. Robots Syst. (IROS)*, Oct. 2022, pp. 9202–9209.

[8] C. J. Kim, X. Yuan, M. Kim, K. S. Kyung, and H. H. Noh, "Monitoring and risk analysis of residual pesticides drifted by unmanned aerial spraying," *Sci. Rep.*, vol. 13, no. 1, p. 10834, Jul. 2023.

[9] R. Sapkota, J. Stenger, M. Ostlie, and P. Flores, "Towards reducing chemical usage for weed control in agriculture using UAS imagery analysis and computer vision techniques," *Sci. Rep.*, vol. 13, no. 1, p. 6548, Apr. 2023.

[10] C. Hiremath, N. Khatri, and M. P. Jagtap, "Comparative studies of knapsack, boom, and drone sprayers for weed management in soybean (Glycine max L.)," *Environ. Res.*, vol. 240, Jan. 2024, Art. no. 117480.

[11] A. Naveed, W. Muhammad, M. J. Irshad, M. J. Aslam, S. M. Manzoor, T. Kausar, and Y. Lu, "Saliency-based semantic weeds detection and classification using UAV multispectral imaging," *IEEE Access*, vol. 11, pp. 11991–12003, 2023.

[12] D. Deng, W. Jing, Y. Fu, Z. Huang, J. Liu, and K. Shimada, "Constrained heterogeneous vehicle path planning for large-area coverage," in *Proc. IEEE/RSJ Int. Conf. Intell. Robots Syst. (IROS)*, Nov. 2019, pp. 4113–4120.

[13] J. Hu, T. Wang, J. Yang, Y. Lan, S. Lv, and Y. Zhang, "WSN-assisted UAV trajectory adjustment for pesticide drift control," *Sensors*, vol. 20, no. 19, p. 5473, Sep. 2020.

[14] Q. Weicai and C. Panyang, "Analysis of the research progress on the deposition and drift of spray droplets by plant protection UAVs," *Sci. Rep.*, vol. 13, no. 1, p. 14935, Sep. 2023.

[15] M. Kamel, S. Verling, O. Elkhatib, C. Sprecher, P. Wulkop, Z. Taylor, R. Siegwart, and I. Gilitschenski, "The voliro omniorientational hexacopter: An agile and maneuverable tiltable-rotor aerial vehicle," *IEEE Robot. Autom. Mag.*, vol. 25, no. 4, pp. 34–44, Dec. 2018.

[16] T. Qing, Z. Ruirui, C. Liping, X. Min, Y. Tongchuan, and Z. Bin, "Droplets movement and deposition of an eight-rotor agricultural UAV in downwash flow field," *Int. J. Agricult. Biol. Eng.*, vol. 10, no. 3, pp. 47–56, 2017.

[17] K. P. Jain and M. W. Mueller, "Flying batteries: In-flight battery switching to increase multirotor flight time," in *Proc. IEEE Int. Conf. Robot. Autom. (ICRA)*, May 2020, pp. 3510–3516.

[18] Y. Wu, X. Du, R. Duivenvoorden, and J. Kelly, "The Phoenix drone: An open-source dual-rotor tail-sitter platform for research and education," in *Proc. Int. Conf. Robot. Autom. (ICRA)*, May 2019, pp. 5330–5336.

[19] G. de Boer, R. Calmer, G. Jozef, J. J. Cassano, J. Hamilton, D. Lawrence, S. Borenstein, A. Doddi, C. Cox, J. Schmale, A. Preußer, and B. Argrow, "Observing the central Arctic atmosphere and surface with University of Colorado uncrewed aircraft systems," *Sci. Data*, vol. 9, no. 1, p. 439, Jul. 2022.

[20] Y. Su, J. Li, Z. Jiao, M. Wang, C. Chu, H. Li, Y. Zhu, and H. Liu, "Sequential manipulation planning for over-actuated unmanned aerial manipulators," in *Proc. IEEE/RSJ Int. Conf. Intell. Robots Syst. (IROS)*, Oct. 2023.

[21] J. Panerati, H. Zheng, S. Zhou, J. Xu, A. Prorok, and A. P. Schoellig, "Learning to fly—A gym environment with PyBullet physics for reinforcement learning of multi-agent quadcopter control," in *Proc. IEEE/RSJ Int. Conf. Intell. Robots Syst. (IROS)*, Sep. 2021, pp. 7512–7519.

[22] J. Liao, C. Liu, and H. H. T. Liu, "Model predictive control for cooperative hunting in obstacle rich and dynamic environments," in *Proc. IEEE Int. Conf. Robot. Autom. (ICRA)*, May 2021, pp. 5089–5095.

[23] HolyBro. (2023). *PX4 User Guide (Main)*. [Online]. Available: https://docs.px4.io/main/en/

RYOSUKE MORISHITA received the B.S. degree from Nihon University, Japan, in 2022. He is currently pursuing the M.S. degree with the University of Tsukuba. His research interest includes UAV.

SHIN KAWAI (Member, IEEE) received the Ph.D. degree from the University of Tsukuba, Japan. He is currently an Assistant Professor with the University of Tsukuba. His research interests include the discretization of systems and digital control.

HAJIME NOBUHARA (Member, IEEE) received the Dr.Eng. degree in computational intelligence from the Tokyo Institute of Technology, Japan, in 2003.

From April 2002 to September 2002, he was a Postdoctoral Fellow with the University of Alberta, Edmonton, Canada. From October 2002 to March 2006, he was an Assistant Professor with the Tokyo Institute of Technology. In 2006, he became an Assistant Professor with the University of Tsukuba and established Computational Intelligence and Multimedia Laboratory. In 2013, he became an Associate Professor with the University of Tsukuba, where he has been a Professor, since 2022. His research interests include computational intelligence, image processing, web intelligence, bioinformatics, and UAV.

● ● ●